# Hybrid Adaptive Robust Control Based on CPG and ZMP for a Lower Limb Exoskeleton

Majid Mokhtari, Mostafa Taghizadeh*⬤ and Mahmood Mazare

*School of Mechanical and Energy Engineering, Shahid Beheshti University, Tehran, Iran*

## SUMMARY
In this paper, hybrid control of central pattern generators (CPGs), along with an adaptive supper-twisting sliding mode (ASTSM) control based on supper-twisting state observer, is proposed to guard against disturbances and uncertainties. Rhythmic and coordinated signals are generated using CPGs. In addition, to overcome the chattering of conventional sliding mode, supper-twisting sliding mode has been applied. The ASTSM method triggers sliding variables, and its derivatives tend to zero continuously in the presence of the uncertainties. Moreover, to acquire maximum stability, the desired trajectory of the upper limb based on zero moment point criterion is designed.

KEYWORDS: Exoskeleton; Adaptive CPG; Adaptive super-twisting sliding mode controller; Super-twisting observer algorithm; ZMP.

## 1. Introduction
Wearable robotic systems (Exoskeletons) are devices that are generally similar to the human body or part of the human body and have harmonious behavior along with the movements of the human body. Exoskeletons are applied to enhance the performance, ability, and potency of healthy human or as a rehabilitation device. Conformity with the human body and also control strategies which are used in exoskeletons has immense impacts on the performance of these means.[1] In 2003, predetermined joint angles of a lower limb exoskeleton robot was controlled, an impedance controller has been used to facilitate a more convenient and user-friendly movement.[2,3] The Blix robot was introduced to increase human strength and endurance in military applications. A model-based control with auxiliary strategy is employed to increase the sensitivity against forces and external torques.[4] To carry out heavy loads for a long periods of time, and for moving on inclined surfaces, a robot called Exo Hicker has been designed, with active control on joint angle.[5] In medical field, to assist people with disabilities to walk, an exoskeleton has been introduced that is controlled based on the pursuit of predetermined joint positions.[6]

Choosing the appropriate control strategy to cope with disturbances, unmodeled dynamics and uncertainties in the system are crucial. Applying the efficient control strategy, the metabolic cost of a person can be reduced by overcoming the disturbances from humans and the environment.

To guard against exogenous disturbances and internal uncertainties, controllers such as feedback linearization, robust and adaptive control, and observer-based controller have been proposed. It should be noted that such control approaches are at highest level but majority of them satisfied relative stabilities.[7] In this state, to track the desired trajectories, control system will spare considerable time. In other words, to ensure that the control law is stable, a great value needs to be chosen for

* Corresponding author. E-mail: mo_taghizadeh@sbu.ac.ir

control gain, which is impractical. Therefore, a robust controller is required with fast convergence for military applications. Nowadays, new control methods have been developed which guarantee the finite-time stability of nonlinear systems, such as Lyapunov finite-time stability approach,[8] terminal sliding mode scheme, and super-twisting sliding mode.[9,10]

Sliding mode control has been developed in recent years as a robust control technique against disturbances and uncertainties.[11,12] Reducing chattering phenomenon which is one of the significant challenges of the sliding mode controller (SMC) leads to save energy. To overcome and mitigate the chattering influences, a boundary layer is defined around the sliding surface which entails detracting the robustness in spite of uncertainties and disturbances.[13]

Super-twisting sliding mode control (STSMC) has been proposed as a new generation of high-order sliding mode control, in which control law inherently and without defining the boundary layer attempts to reduce the chattering phenomenon, while keeping the ability of conventional sliding controller to deal with uncertainties and disturbances.[14] Super-twisting sliding mode (STSM) is one of the most vigorous second-order continuous SMCs. This control method produces a continuous control function which obliges sliding variables, and its derivatives tend to zero in finite time in the presence of disturbances with restricted amplitude. Since this control method has a discrete integral, the chattering phenomenon is not eliminated but is reduced to a satisfactory level.[15] The basis of this control methodology was presented by Mornova and Serio in 2008.[16] It was used in the wind turbine system[17] and accurate control of the rotor position and the estimation of the stator resistance of a synchronous magnetic machine.[18]

In sliding mode control, knowing the range of uncertainties and disturbances is a fundamental flaw and in many cases is not measurable. An adaptive super-twisting sliding mode (ASTSM) control law is as an efficient method for dealing with disturbances with unknown amplitude. Significant properties of this method are precise tracking within finite time, reducing mechanical stresses, and coping with the chattering phenomenon without requiring the output derivatives, high resistance to uncertainties and internal and external disturbances, and relatively simple control laws that can be designed based on nonlinear models.

How to determine the desired trajectories of robot joints has been another important issue in lower limb exoskeleton. Central pattern generator (CPG) is one of the online and robust methods against environmental disturbances for designing the desired trajectories of exoskeletons. In many biological systems such as breathing, base motion patterns are generated by CPG. The CPGs include neural networks which can produce rhythmic and coordinated signals for controlling the motion of legged robots.[20]

CPG models are also among approaches for online trajectory generation that have been repeatedly employed in different robotic applications, for example, snake-like robots,[21] Quadruped Robots,[22] swimming salamander robot[23] and exoskeleton robots.[24]

CPGs are a collection of coupled nonlinear oscillators that can encode periodic input signals as limit cycles of oscillators.[25] The walking pattern is usually set by the parameters of the CPG which allows altering the walking characteristics, such as frequency and amplitude. The use of CPGs and also various oscillators in robotics are expressed in Refs. [26,27]. CPG for controlling motion systems has many advantages, such as providing stable moron patterns and quick return to normal and rhythmic behavior in case of disturbances in the system. Also, the utilization of feedback signals makes it possible for CPGs to create flexible movements in unknown environments.[26] To optimize the CPG parameter, including the parameters of each oscillator and the weight of the coupling between them, evolutionary algorithms are applied.[28–30]

Hybrid CPG and controller or movement characteristics of the robot such as stability have been applied in order to ameliorate exoskeleton performance and also boom the controllability of such devices.[15–25]

Stability is one of the crucial duties of walking mechanisms during gaiting. Center of mass stability,[31] energy-based stability,[32] and zero moment point (ZMP) criterion are the most important stability criteria in this realm.[33] If the robots have active joints, and in each moment stand on one leg, ZMP can be applied regarding stability assessment. This criterion was taken into account for the bipedal robot in Vasda University and then has been widely employed. In many researches, to guarantee stability during gaiting process, well-suited trajectories are designed for upper limb joint based on ZMP.[34]

Table I. Parameters of lower limb exoskeleton robot.

| Parameter | Units | Values | Parameter | Units | Values | Parameter | Units | Values |
|---|---|---|---|---|---|---|---|---|
| $m_1$ | kg | 1 | $I_3$ | kg m$^2$ | 1 | $L_5$ | m | 0.5 |
| $m_2$ | kg | 3 | $I_4$ | kg m$^2$ | 2 | $L_7$ | m | 0.2 |
| $m_3$ | kg | 5 | $I_5$ | kg m$^2$ | 1 | $r_1$ | m | 0.1 |
| $m_4$ | kg | 10 | $I_6$ | kg m$^2$ | 0.6 | $r_2$ | m | 0.25 |
| $m_5$ | kg | 5 | $I_7$ | kg m$^2$ | 0.2 | $r_3$ | m | 0.25 |
| $m_6$ | kg | 3 | $L_1$ | m | 0.2 | $r_4$ | m | 0.25 |
| $m_7$ | kg | 1 | $L_2$ | m | 0.5 | $r_5$ | m | 0.25 |
| $I_1$ | kg m$^2$ | 0.2 | $L_3$ | m | 0.5 | $r_6$ | m | 0.25 |
| $I_2$ | kg m$^2$ | 0.6 | $L_4$ | m | 0.5 | $r_7$ | m | 0.1 |

In this paper, an exoskeleton dynamic model is extracted using the Lagrange method. In order to control the robot and ensure stable walking, a hybrid method comprising an adaptive CPG (based on Vander Pol oscillators) and an adaptive super-twisting sliding mode controller (CPG-ASTSMC) is proposed to effectively deal with the disturbances and uncertainties as well as a quick return to the correct walking pattern. Also, the motion of upper limb joint is used as compensator to achieve robot stability based on ZMP. The joints variables are estimated at each moment by using a super-twisting observer. Moreover, in order to acquire maximum stability and minimum tracking error, the parameters of the proposed controller and the upper limb desired trajectory are optimized using Harmony Search Algorithm (HSA).[35] In the next step, the proposed controller performance is compared to the proposed method in Ref. 25, in which control command is generated using only the CPG algorithm, as well as the hybrid method including the adaptive CPG algorithm and an optimal adaptive SMC (CPG-SMC).

The structure of the paper is organized as follows: In Part 2, an exoskeleton robot is introduced and the dynamic model is extracted using the Lagrange method. In Section 3, the control method is presented and its stability is investigated. In Section 4, the desired trajectory for the upper limb is determined to achieve the highest system stability based on ZMP criteria. In Section 5, the proposed controller has been applied to the extracted model of the Lagrange method in order to track the desired trajectories of the joints and finally, and conclusion is presented in Section 6.

## 2. Introduction and Modeling of Understudied Mechanism
Kinematic compatibility of the degrees of freedom (DOFs) with human body and strict conformity between robot joints and human joints oblige the kinematics of the robot to follow the user's kinematics completely, which solves many design problems. This approach has been used in designing Hall series.[36,37] The understudied model in this paper is a lower limb exoskeleton robot containing seven links and five active joints for the hip, knee, and ankle of the left and right legs. In Fig. 1, the schematic of this robot is shown.

In Fig. 1, $\theta_i$ for $i = 1, 2, \ldots, 7$ is the absolute angle of each joint, $q_i$ is the relative angle of each joint and $I_i$ is the moment of inertia of the links. By extracting the kinematic relationships and using the Lagrange method, the dynamic model of the robot is expressed as Eq. 1.[38]

$$\tau = M(\theta)\ddot{\theta} + C(\theta, \dot{\theta}) + G(\theta) + \tau_d \tag{1}$$

where $\tau$ is the torque vector of the actuators, $M(\theta)$ is the inertia moment matrix, $C(\theta, \dot{\theta})$ is the centrifugal and gyroscopic effects matrix, $G(\theta)$ is the vector of gravitational forces, and $\tau_d$ is the disturbance torque. The parameters of lower limb exoskeleton robot are shown in Table I.[40]

### 2.1. Distinct phases of walking gait
A single gait of motion is divided into two phases, a single-support phase (SSP) and then a double-support phase (DSP). Immediately after each phase, the robot receives an impulse in contact with the ground. The simplified steps of one gait of walking are shown in Fig. 2.

In the first phase (Fig. 2(a)), the robot motion is considered as a 5-DOF motion on two supports (the front heel and the rear paw). The holonomic constraints associated with this constrained motion are applied in the simulation.
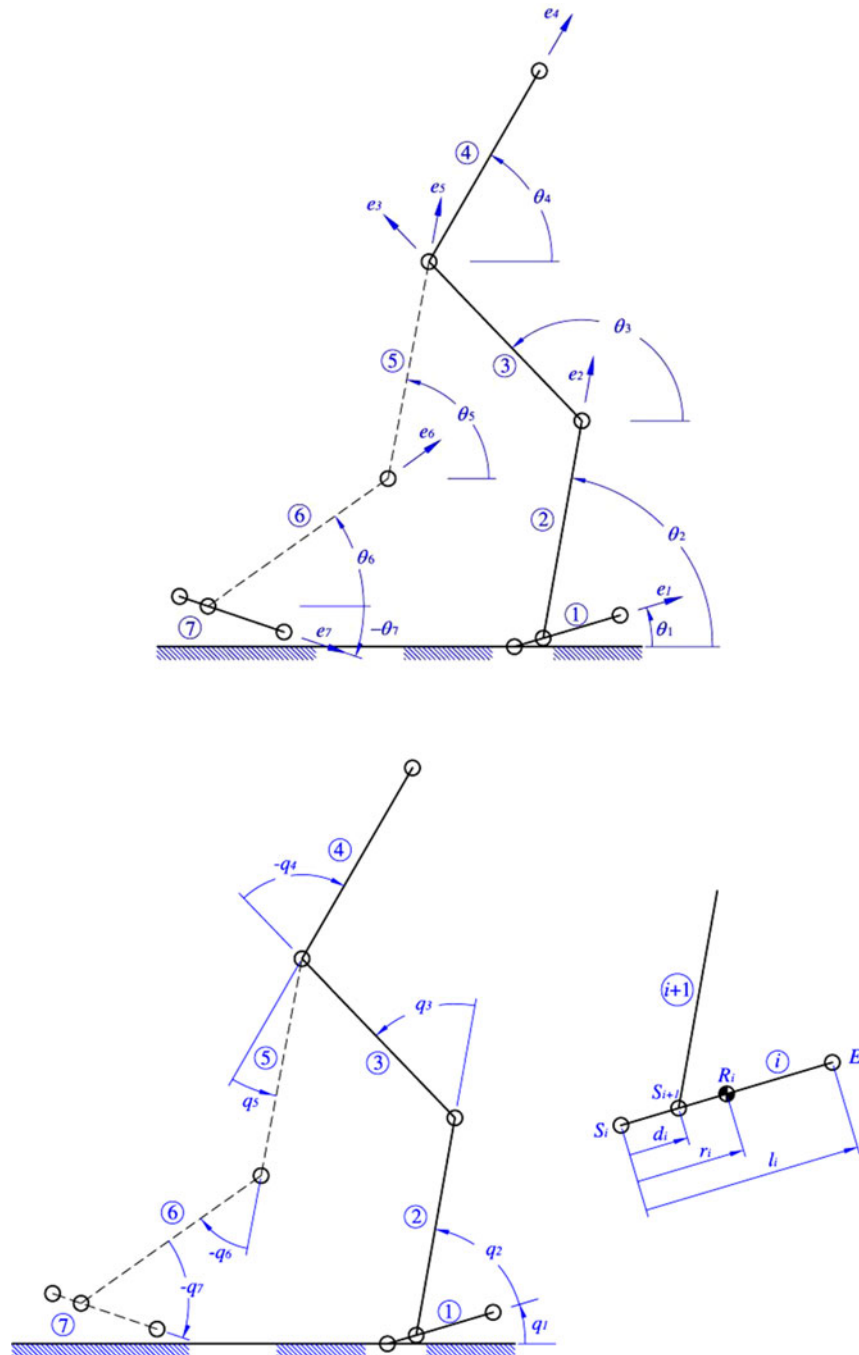
Fig. 1. Schematic of a 7-DOF lower limb exoskeleton.

At the end of the first phase (Fig. 2(b)), impact of the front paw is occurred with the ground in an instance and simultaneously the rear foot loses its contact with the ground.

In the second phase (Fig. 2(c)), the robot motion is considered as a 7-DOF motion on a single support (fixed foot) and it is simulated as an unconstrained motion.

At the end of the second phase (Fig. 2(d)), impact of the front foot heel is occurred with the ground and simultaneously the heel of the opposite foot lifts from the ground.

*2.1.1. Impact model.* The impact at the end of each phases is modeled like an impact between two rigid bodies. Using well-suited hypothesizes, the velocity of generalized coordinates can be determined after impact based on the velocity of the coordinates before impact. It should be noted that, all
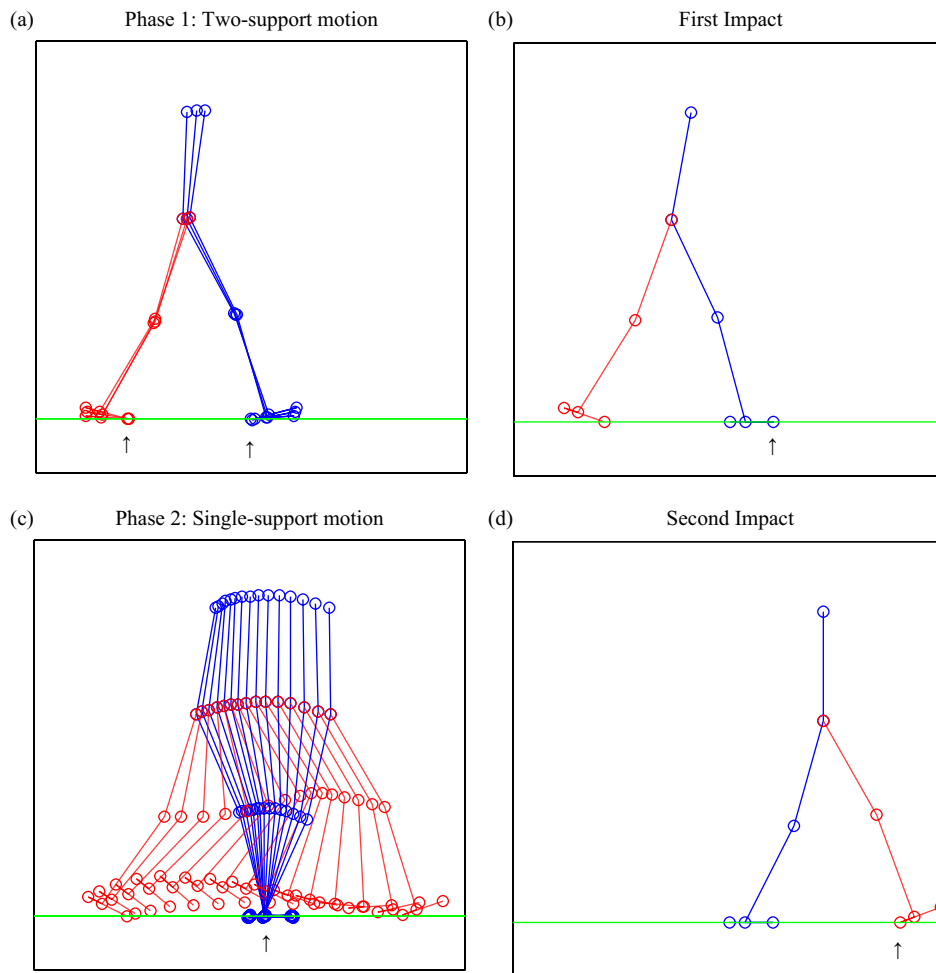
Fig. 2. Motions phases and impact instances: (a) double-support phase, (b) paw impact, (c) single-support motion phase, and (d) heel impact.

of the DOFs should be considered for impact modeling. It is assumed that during impact, rebound and slipping will not occur and stance leg lifts from the ground without any interaction. In the next, the following hypotheses have been taken into account:

- The impacts are instantaneous.
- The external force acting on the model during the impact is considered impulsive.
- The impulsive force causes instantaneous change in the generalized velocities, while there is no change in positions.
- All of the applied torques on the joints of the robot are not impulsive.
- The impact is fully plastic.

Under the abovementioned hypotheses, by integrating from Eq. (1) over the impact duration:

$$\boldsymbol{M}(q)\left(\dot{q}^{+} - \dot{q}^{-}\right) = \int_{t^{-}}^{t^{+}} \delta F_{\text{ext}}(\tau) d\tau = J_{2}^{T} \lambda \tag{2}$$

where $\dot{q}^{-}$ and $\dot{q}^{+}$ are the velocities just before and after the impact. According to the third hypothesis, the positions do not experience any change during the impact, and thereby $q^{+} = q^{-}$. Moreover, $J$ is the Jacobean of the swing leg's coordinates, which is obtained using kinematic equation of the leg.

Two other equations can be extracted using geometric conditions in the impacts' point. Based on the impact hypotheses, the external forces applied to stance leg are equal to zero due to the fact that the leg in impact lifts from the ground instantaneously. Hence, it seems necessary to consider

exogenous forces on the bottom of swing leg. The two required equations can be written based on no slip and no rebound hypothesis:

$$\dot{x}_p^+ = 0, \dot{y}_p^+ = 0 \tag{3}$$

where $x_p$ and $y_p$ are the coordinates of the impact point of the robot.

So,

$$J_2(q)\dot{q}^+ = 0 \tag{4}$$

Equations (2–4) can be solved for $\lambda$ and $\dot{q}^+$, so the generalized velocities after impact ($\dot{q}^+$) can be determined knowing those ($\dot{q}^-$) before it.

## 3. Hybrid Control System

In this paper, a hybrid method including CPG algorithm and ASTSMC has been applied for tracking the desired trajectories in the presence of disturbances and uncertainties and also generating a soft and stable motion for the exoskeleton.

### 3.1. Central pattern generator

Wearable robotic systems such as lower limb exoskeletons do not only provide effective and repetitive gait training but also reduce the burden of physiotherapists. This is because it allows the integration of the human intelligence with that of the mechanical power of the robot. Among other applications, these devices may be required for gait rehabilitation and human locomotion assistance. Rehabilitation via exoskeletons is of great importance to people with lower limb disorders. For any exoskeleton to perform its required function, it has to be equipped with some form of control mechanism. Initiating a control mechanism involves generating a reference input signal which is expected to go through the controller in order to produce the control signal necessary to drive the actuators of the exoskeleton. In gait rehabilitation and human locomotion assistance, the wearer depends almost solely on the torque generated by the exoskeleton device. This is because the joint torque generated by the muscles of the wearer is either infinitesimally small or zero. Generating a reference input (desired motion) signal does not have to be arbitrary since it has to suit the natural envisaged motion (nerve signals) of the wearer developed by the brain. This does give rise to the use of CPGs to produce such signal that is closely related to the nerve signals.

CPG can be defined as a neural network which is able to generate rhythmic patterns intrinsically or as a neural circuit to produce periodic commands for rhythmic behaviors like locomotion. In this regard, a wide variety of neural oscillators such as Vander Pol, Hopf, Wilson-Cowan, and Matsuoka oscillators have been applied to create CPG and also desired trajectories.[25,26] It should be noted that the main ambition of CPG stemming from the behavioral pattern of the oscillatory neural networks and also stable rhythmic pattern. In this paper, a network of coupled Vander Pol oscillators is applied to determine the desired angles of ankle, knee, and hip of both left and right legs. In following, the differential equations of coupled Vander Pol oscillators for generating the walking trajectory are introduced.[39]

$$\ddot{x}_1 - \mu_1\left(p_1^2 - x_a^2\right)x_1 + g_1^2 x_a = \varphi_1$$
$$\ddot{x}_2 - \mu_2\left(p_2^2 - x_b^2\right)x_2 + g_2^2 x_b = \varphi_2$$
$$\ddot{x}_3 - \mu_3\left(p_3^2 - x_c^2\right)x_3 + g_3^2 x_c = \varphi_3$$
$$\ddot{x}_4 - \mu_4\left(p_4^2 - x_d^2\right)x_4 + g_4^2 x_d = \varphi_4$$
$$\ddot{x}_5 - \mu_5\left(p_5^2 - x_e^2\right)x_5 + g_5^2 x_e = \varphi_5$$
$$\ddot{x}_6 - \mu_6\left(p_6^2 - x_f^2\right)x_6 + g_6^2 x_f = \varphi_6 \tag{5}$$

where $x_i$ is the output signal, $p_i^2$ represents the amplitude, $g_i^2$ refers to the frequency, $\varphi_i$ is the offset parameter, $\mu_i$ indicates the nonlinearity and the damping strength, while $x_{a-f}$ is the coupling equations and mathematically written as
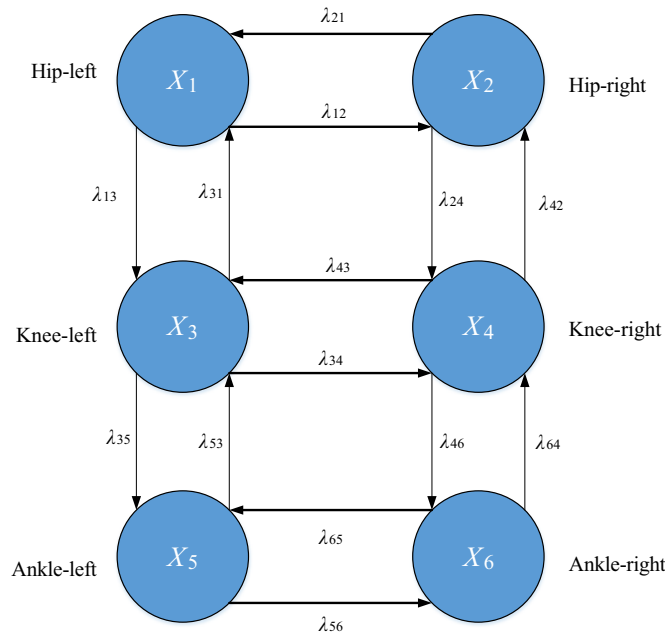
Fig. 3. Nature of coupling between the oscillators.

$$x_a = x_1 - \lambda_{21}x_2 - \lambda_{31}x_3$$

$$x_b = x_2 - \lambda_{12}x_1 - \lambda_{42}x_4$$

$$x_c = x_2 - \lambda_{13}x_1 - \lambda_{31}x_4 - \lambda_{53}x_5$$

$$x_d = x_4 - \lambda_{24}x_2 - \lambda_{34}x_4 - \lambda_{64}x_6$$

$$x_e = x_5 - \lambda_{35}x_3 - \lambda_{65}x_6$$

$$x_f = x_6 - \lambda_{46}x_4 - \lambda_{56}x_5 \tag{6}$$

with $\lambda_{ij}$ (i $\neq$ j) refers to the coupling coefficient. Moreover, the coupling of the networked oscillators is depicted in Fig. 3.

In this paper, CPG parameters are optimized by HSA to minimize the error function of the Eq. (7), in order to create a smooth and stable motion.

$$\text{cost function} = \int_0^t (\theta_{\text{Real-Time}} - \theta_{\text{Desired}}) \, dt \tag{7}$$

In Eq. (7), $\theta_{\text{Desired}}$ is generated desired trajectory based on CPG and $\theta_{Real-Time}$ is the trajectory from real-time measurement of each joint.

### 3.2. Adaptive-gain STSMC

In this section, an adaptive-gain STSMC for the system is designed. Sliding mode control is one of the control methods in the category of robust controllers.[23] In order to design an SMC, for each state variable (q), the error is considered to be $e = q - q_d$ and a sliding variable is defined in accordance with equation (8). For each state variable,

$$S(q, t) = \left( \frac{d}{dt} + \lambda \right)^{n-1} e \tag{8}$$

where $\lambda$ is a definitely positive constant and *n* is the state space, which is equal to 3 for the robot being studied. The SMC sets the derivative of the sliding variable near zero. Eq. (9) is obtained by deriving a sliding variable relative to time.

$$\dot{S} = (\ddot{q} - \ddot{q}_d) + (\dot{q} - \dot{q}_d) \tag{9}$$

Setting the derivative of the sliding variable to zero and using Eq. (1), the control rule $\tau\tau(t)$ is obtained as Eq. (10).

$$\hat{\boldsymbol{\tau}}(t) = \boldsymbol{C}\left(\theta, \dot{\theta}\right) + \boldsymbol{G}(\theta) + \boldsymbol{M}(\ddot{q}_d - (\dot{q} - \dot{q}_d)) + \boldsymbol{\tau_d} \tag{10}$$

Chattering phenomenon is one of the main disadvantages of the sliding mode control, which increases energy consumption. In order to cope with this phenomenon, a discontinuous term is added as a boundary layer to the control rule. Finally, the control law is extracted in Eq. (11).

$$\boldsymbol{\tau}(t) = \hat{\boldsymbol{\tau}}(t) - K_{\text{sign}}(\boldsymbol{S}) \tag{11}$$

where in Eq. (11), $K$ is a positive constant. Using the boundary layer to eliminate the chattering phenomenon not only does not completely eliminate this phenomenon but also reduces the robustness characteristics of the controller. STSM controller is a well-suited approach to eliminate the chattering phenomenon without reducing the robustness characteristics of the controller. The STSM method is suitable for confronting disturbances and uncertainties with a known and limited range.[39] Defining a range of uncertainties and disturbances is usually sophisticated or impossible. Hence, ASTSM method is presented as an effective way to eliminate disturbances and uncertainties with unknown range. Finally, the adaptive-gain super-twisting sliding mode control law is designed by adding $\omega$ to Eq. (11).[41]

$$\boldsymbol{\tau_i}(t) = \hat{\boldsymbol{\tau}}_i(t) + \omega_i$$

$$\omega_i = A_i\sqrt{|S_i|}\text{sign}(\boldsymbol{S}) + \vartheta_i$$

$$\dot{\vartheta}_i = -\frac{\beta_i}{2}\text{sign}(\boldsymbol{S}) \tag{12}$$

In Eq. (12), $\beta = 2\varepsilon A$ and also

$$\dot{A} = \begin{cases} w_1\sqrt{\frac{\gamma_1}{2}}\text{sign}\left(|\boldsymbol{S}| - \mu\right) & A > \alpha_m \\ \eta & A > \alpha_m \end{cases} \tag{13}$$

where $w_1$, $\gamma_1$, $\varepsilon$, $\mu$, and $\eta$ are constant. In order to indicate stability of the control method, positive Lyapunov function is considered as Eq. (14).[16]

$$V_i = \delta_i^T P_i \delta_i \tag{14}$$

$$\delta_i = \begin{bmatrix} \sqrt{|\boldsymbol{S}_i|}\text{sign}\left(\boldsymbol{S}_i\right) & \vartheta_i \end{bmatrix}^T \tag{15}$$

$$P_i = \begin{bmatrix} -\frac{4\beta_i}{2} + A_i^2 & -A_i \\ -A_i & 2 \end{bmatrix} \tag{16}$$

By taking time derivative and also some mathematical simplification,

$$\dot{V}_i = -\frac{1}{\sqrt{|\boldsymbol{S}_i|}}\left(\delta_i^T Q_i \delta_i + \tau_{di}q_i^T \delta_i\right) \tag{17}$$

$$Q_i = \frac{1}{2}\begin{bmatrix} -\frac{4\beta_i}{2} + A_i^2 & -A_i \\ -A_i & 1 \end{bmatrix} \tag{18}$$

$$q_i^T = -\frac{4\beta_i}{2} + \frac{A_i^2}{2} - \frac{A_i}{2} \tag{19}$$

Substituting $Q_i$ and $qq_i^T$ in $\dot{V}_i$:

$$\dot{V}_i = -\frac{1}{\sqrt{|S_i|}} \left( \delta_i^T \hat{Q}_i \delta_i \right) \tag{20}$$

$$\hat{Q}_i = \frac{1}{2} \begin{bmatrix} -\frac{4\beta_i}{2} + A_i^2 - \left(\frac{8\beta_i}{A_i} + A_i\right)\Delta_i & -A_i - 2\Delta_i \\ -A_i - 2\Delta_i & 1 \end{bmatrix} \tag{21}$$

$$A_i > 2\Delta_i, \quad -\frac{\beta_i}{2} > A_i \frac{5A_i\Delta_i}{2A_i - 4\Delta_i} \tag{22}$$

If condition (22) is satisfied, $\dot{V}_i$ is negative and thereby stability of the closed loop system is guaranteed.

### 3.3. Estimate the system state with a super-twisting algorithm

In exoskeleton systems, although coordinates of each joint may be measured accurately by an encoder, sensing velocity by tachometers can encompass noises. Furthermore, numerical integration and derivation of sensor data such as gyroscopes and accelerometers, as well as sensor noise, can cause a significant error in the control loop. Therefore, to overcome such challenges, a state estimator algorithm has always been considered. In this study, a super-twisting algorithm is applied to estimate system states[16] which proposed by Levant.[42,43]

$$\dot{\hat{q}}_{1i} = \hat{q}_{2i} + z_{1i}$$

$$\dot{\hat{q}}_{2i} = M^{-1}(q_{1i})\left(\tau - C\left(q_{1i}, \dot{\hat{q}}_{2i}\right) - G(q_{1i}) - \tau_d\right) + z_{2i} \tag{23}$$

In Eq. (23), $\hat{q}_{1i}$ and $\hat{q}_{2i}$ are the estimated states. $z_{1i}$ and $z_{2i}$ are the correction variables of the output errors that are added to the estimation equations.

$$z_{1i} = \gamma\sqrt{|\hat{q}_{1i} - \hat{q}_{2i}|}\,\text{sign}\left(q_{1i} - \hat{q}_{1i}\right)$$

$$z_{2i} = k\,\text{sign}\left(q_{1i} - \hat{q}_{1i}\right) \tag{24}$$

In Eq. (24), $\gamma$ and k are constants. The estimation error can be considered as

$$e_{1i} = q_{1i} - \hat{q}_{1i}$$

$$e_{2i} = q_{2i} - \hat{q}_{2i} \tag{25}$$

By considering the estimation errors in the form of Eq. (25), the error estimation equations can be written as Eq. (26).

$$e_{1i} = e_2 - \gamma\sqrt{|e_{1i}|}\,\text{sign}\,(e_{1i})$$

$$e_{2i} = M^{-1}(q_{1i})\left(-C(q_{1i}, \dot{q}_{2i}) - G(q_{1i})\right) - M^{-1}(\hat{q}_{1i})\left(-C\left(\hat{q}_{1i}, \dot{\hat{q}}_{2i}\right) - G(\hat{q}_{1i})\right) \tag{26}$$

$$- k\,\text{sign}\,(e_{1i}) - M^{-1}(q_{1i})\tau_d$$

## 4. Upper Limb Joint Trajectory Based on ZMP Stability Criterion

Another significant issue associated with stability of biped robot is ZMP which should be considered. The ZMP is a point on the ground in which sum of all the active force moments is equal to zero. If the ZMP perches into the support polygon between the foot and the ground, stability of the biped

Table II. Values of oscillators parameters.

| Parameters | Symbol/value | | | | | |
|---|---|---|---|---|---|---|
| Damping srength | $\mu_1$ | $\mu_2$ | $\mu_3$ | $\mu_4$ | $\mu_5$ | $\mu_6$ |
| | 2 | 1 | 1.5 | 1.5 | 1 | 2 |
| Amplitude | $p_1^2$ | $p_2^2$ | $p_3^2$ | $p_4^2$ | $p_5^2$ | $p_6^2$ |
| | 1.5 | 2 | 1 | 1 | 2 | 1.5 |
| Frequency | $g_1^2$ | $g_2^2$ | $g_3^2$ | $g_4^2$ | $g_5^2$ | $g_6^2$ |
| | 15 | 28 | 15 | 15 | 28 | 15 |
| Offset | $\varphi_1$ | $\varphi_2$ | $\varphi_3$ | $\varphi_4$ | $\varphi_5$ | $\varphi_6$ |
| | 3 | −2 | 10 | 10 | −2 | 3 |
| Coupling coefficients | 21 | 12 | 31 | 13 | 24 | 42 |
| | 0.3 | 0.3 | 0.3 | 0.3 | 0.3 | 0.3 |
| | 35 | 53 | 46 | 64 | 65 | 56 |
| | 0.3 | 0.3 | 0.3 | 0.3 | 0.3 | 0.3 |
| | 34 | 43 | | | | |
| | 0.3 | 0.3 | | | | |
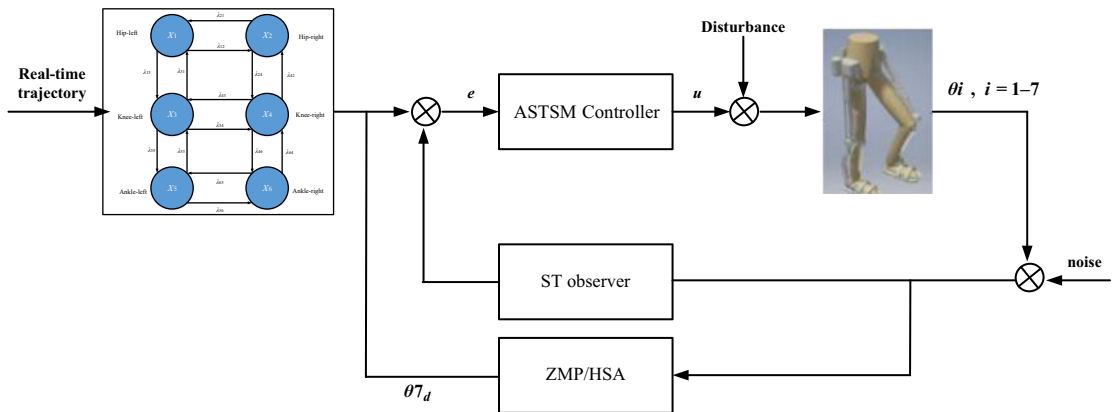


Fig. 4. Block diagram of the proposed scheme.

robot is guaranteed.[44] Therefore, instability of the robot can be illustrated through monitoring the ZMP location. The ZMP in *x*-axis direction can be calculated as follows:

$$x_{ZMP} = \frac{\sum_{i=1}^{n} m_i (\ddot{z}_i + g) x_i - \sum_{i=1}^{n} m_i \ddot{x}_i z_i - \sum_{i=1}^{n} I_{iy} \ddot{\theta}_{iy}}{\sum_{i=1}^{n} m_i (\ddot{z}_i + g)}$$

$$y_{ZMP} = \frac{\sum_{i=1}^{n} m_i (\ddot{z}_i + g) y_i - \sum_{i=1}^{n} m_i \ddot{y}_i z_i - \sum_{i=1}^{n} I_{ix} \ddot{\theta}_{ix}}{\sum_{i=1}^{n} m_i (\ddot{z}_i + g)} \qquad (27)$$

where *y* and *z* are the robot center of mass coordinates, respectively, and $\ddot{\theta}_{ix}$ and $\ddot{\theta}_{iy}$ are angular acceleration of robot links in vertical and horizontal directions, respectively. In this research, to stability compensation, upper limb motion is neglected, and for doing this, the desired trajectory of the joint is determined so that ZMP criterion is checked in each moment. The angles, velocities, and angular acceleration of the joint are obtained based on satisfying ZMP in every moment. The desired trajectory of upper limb is introduced using a five-order spline, embodies a couple of accurate points in one walking gait, and then trajectories parameters are optimized by minimizing an objective function. Moreover, to contribute and strengthen the stability of the robot using ZMP, an objective function
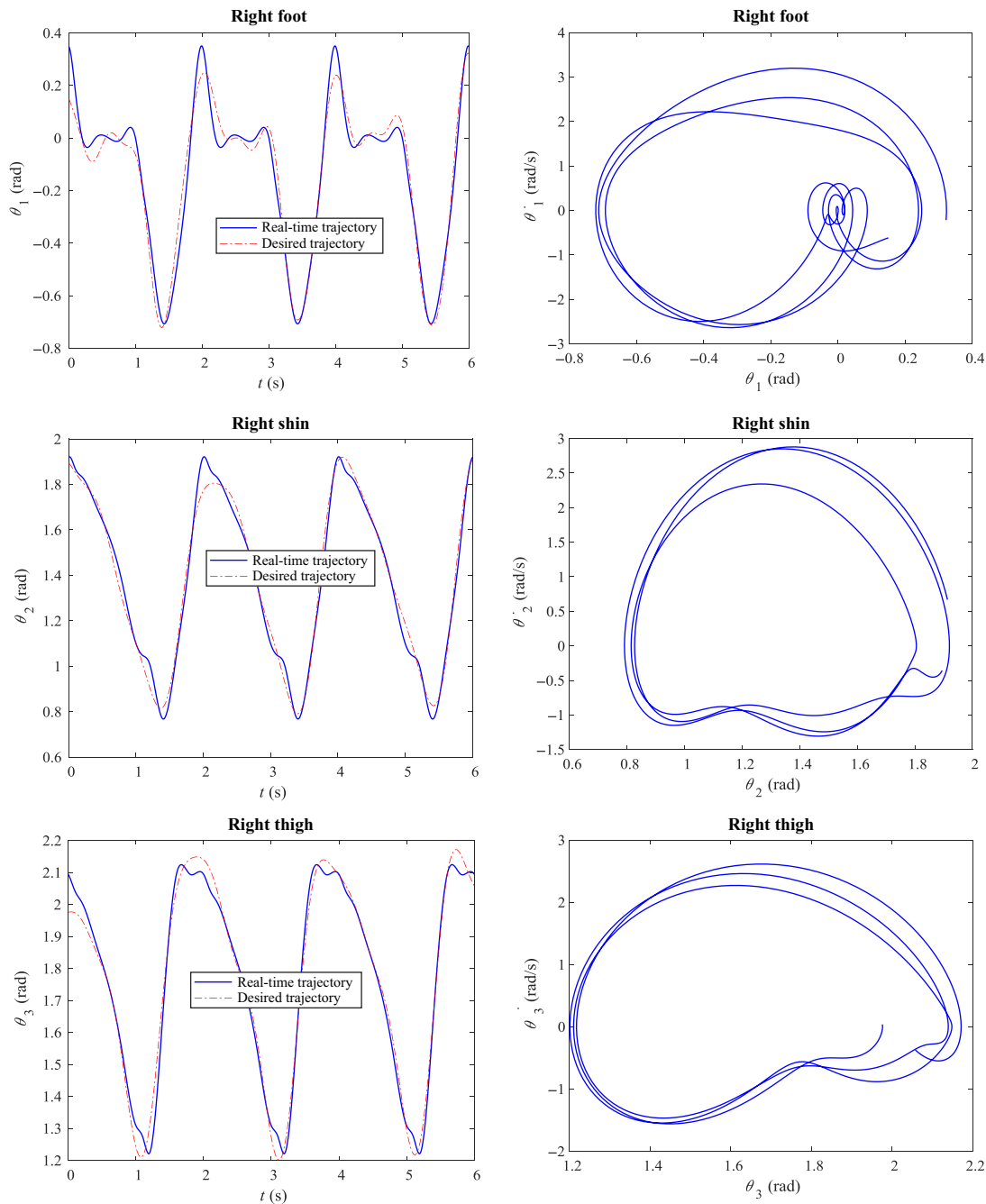
Fig. 5. Stable limit cycle in phase plane and desired trajectories.

is considered so that will be able to create the maximum stability margin and minimum deviation between joint trajectories and reference trajectories in every moment.

$$CF = \int |ZMP - ZMP_{\text{desird}}|^2 + \sum_{i=1}^{7} \int |e_i|^2 \tag{28}$$

where $ZMP_{\text{desird}}$ is the ZMP in SSP and DSP which is defined based on maximum stability value in each phase and $e_i$ is the trajectory tracking error. To have proportional movement between the robot and user, the authorize range for upper limb joint is chosen as $75° \leq \theta \leq 115°$. Block diagram of the proposed scheme is portrayed in Fig. 4.
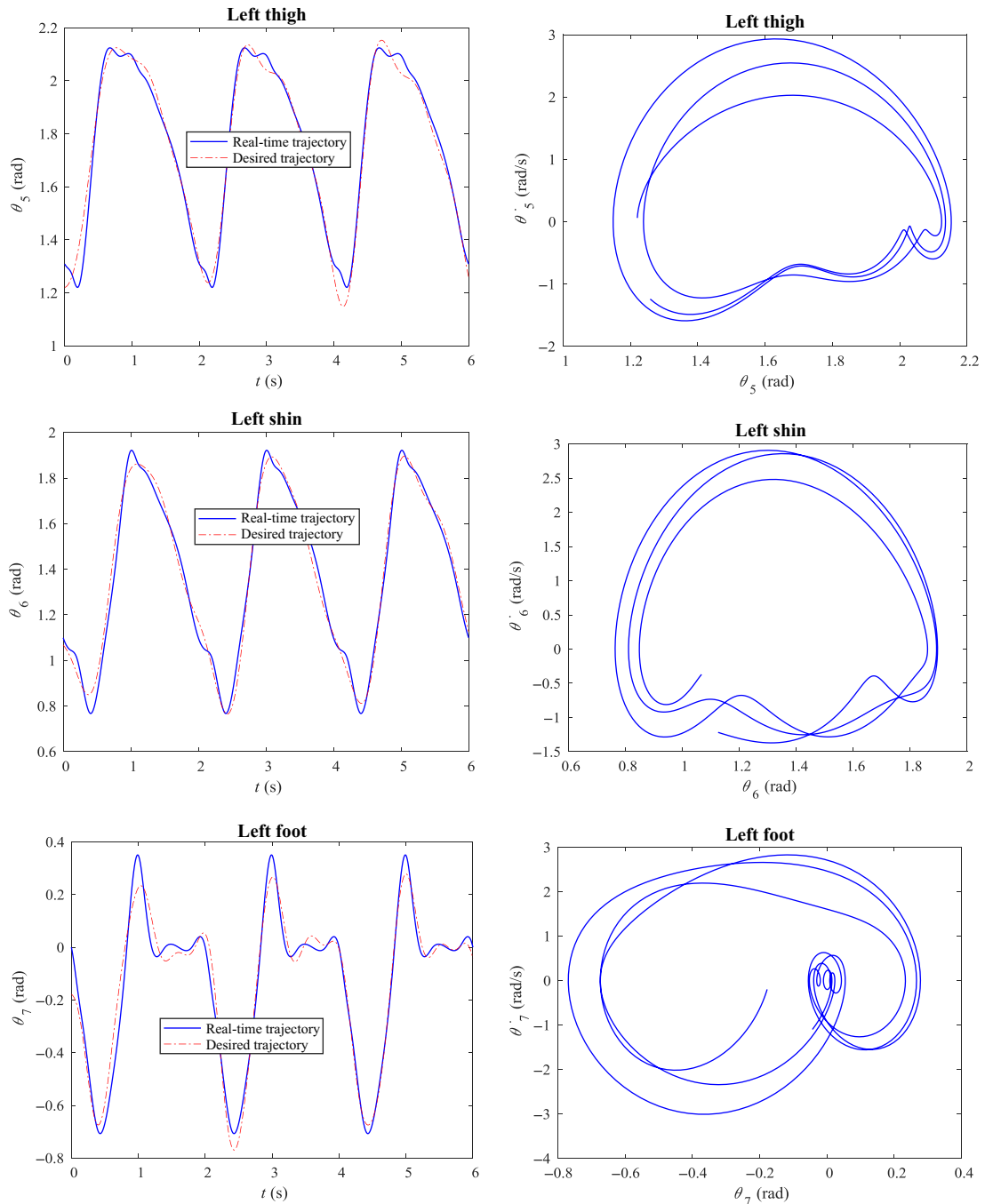
Fig. 5. Continued.

## 5. Simulation Results

In this section, simulations are performed to reveal the effectiveness of the proposed adaptive-gain supper-twisting SMC in tracking the joints position. To do this, desired stable trajectories are generated by CPG based on real-time sampling data of actual walking. The joints variables are estimated at each moment by using a super-twisting observer. It should be noted that to achieve high level of stability for upper limb, its desired trajectory is designed based on ZMP criterion. Also, to indicate the robustness of the designed controller, parametric uncertainties and time-varying disturbances are considered in all simulations.

CPG parameters are optimized by HSA to minimize the error function of the Eq. (4), in order to create a smooth and stable motion. The CPG parameters are shown in Table II. Stable limit cycle
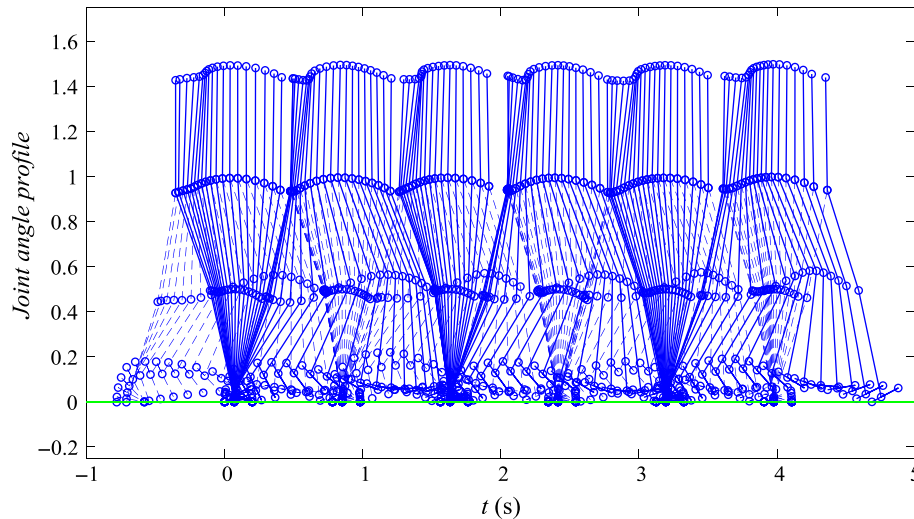
Fig. 6. Stick diagram of joint angles profile evolution.

in phase plane and also generated desired trajectories based on CPG and the data from real-time measurement of each joint from a rehabilitation clinic are compared in Fig. 4.

Figure 5 shows that a set of coupled oscillators can create a suitable trajectory similar to the reference trajectory for each joint. The results produced by the CPGs are applied to the robot on line, to create movements that are smooth, continuous, and robust against disturbances. A human gait cycle consists of the stance and swing phase which is divided into the SSP and the DSP. Periodic sequence is one of the most amazing characteristics of the rhythmic pattern for trajectories of the exoskeleton. The automatic transmission between two distinct phases, SSP and DSP, in fast sequence via the stick diagram is depicted in Fig. 6.

Desired trajectory generated by CPG has a strict conformity with experimental data, which reveals the outperforming of the coupled oscillators in CPG procedure.

The controller is then implemented to the robot over the designed trajectories, and simulation results are obtained. Also, to indicate the robustness of the designed controller, parametric uncertainties and time-varying disturbances are considered in all simulations. To optimize two controllers and upper limb joint parameters, an objective function (Eq. 25) is considered which minimized using HSA. The CPG-SM method and the CPG-ASTSM method are applied to the robot. Figure 6 illustrates how the robot tracks the paths produced by CPG for each joint by using the CPG-ASTSM method provided. In all of the control methods presented, estimates of system state variables are accomplished using a super-twisting algorithm.

Figure 7 shows the proper tracking of trajectories designed by CPG method by ASTSMC. In order to indicate observer performance in estimation of system states, the control command generated by ASTSMC and estimated control command are shown in Fig. 8, which demonstrates the capability of the estimation rule by super-twisting algorithm.

Figure 8 represents the proper performance of the super-twisting algorithm in estimating the position of the joints. The control signals generated by the CPG-ASTSMC method are in the right amount to apply to the operators.

The proposed controller performance is compared with the proposed method in Ref. 25. To demonstrate the performance of the proposed controller, two criteria as the integral of the absolute squared of the error (IASE) and the root mean square (RMS) of the absolute signal control for different controller have been investigated. IASE error criteria are considered which are defined in the Eq. (29).

$$IASE = \int |e(t)|^2 \, dt \tag{29}$$

The IASE and RMS of the control signal are mentioned in Table III to compare performance of the three methods, CPG-SM, ASTSMC, and CPG-ASTSM.
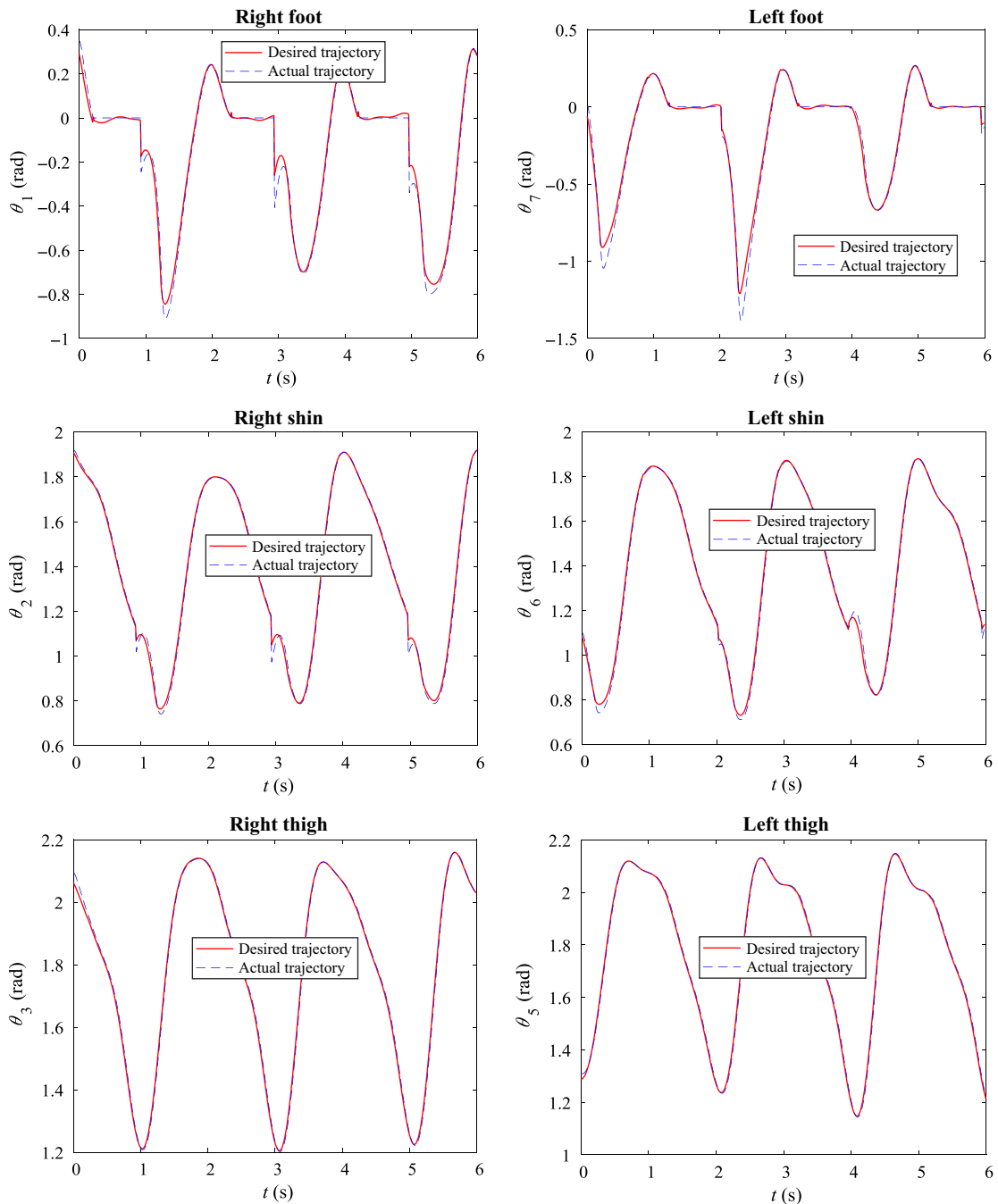
Fig. 7. Trajectory tracking of each joint using CPG-ASTSMC.

Based on IASE, it is worth mentioning that CPG-ASTSMC has less tracking error rather than CPG-SMC. High convergence rate is one of the most characteristics of the ASTSMC in practical applications. Moreover, control input RMS reveals the influence of CPG when hybrid by ASTSMC, and the control command of the CPG-SMC has tremendous chattering while due to natural behind of ASTSMC, the phenomenon has been eliminated. It should be noted that upper limb joint trajectory is designed based on ZMP in order to achieve maximum stability which is depicted in Fig. 9. In addition, ZMP is portrayed in Fig. 10.

According to Fig. 10, three methods can create stable motion for the robot using the movement of upper limb, so that the ZMP generated trajectory by CPG-ASTSMC has a smaller deviation with desired ZMP trajectory and thus will cater a higher stability margin. The overriding issue resides in accuracy and resolution of the CPG-ASTSMC in tracking the reference trajectories of robot joints

Table III. Different criterions for comparing the performance of the controllers.

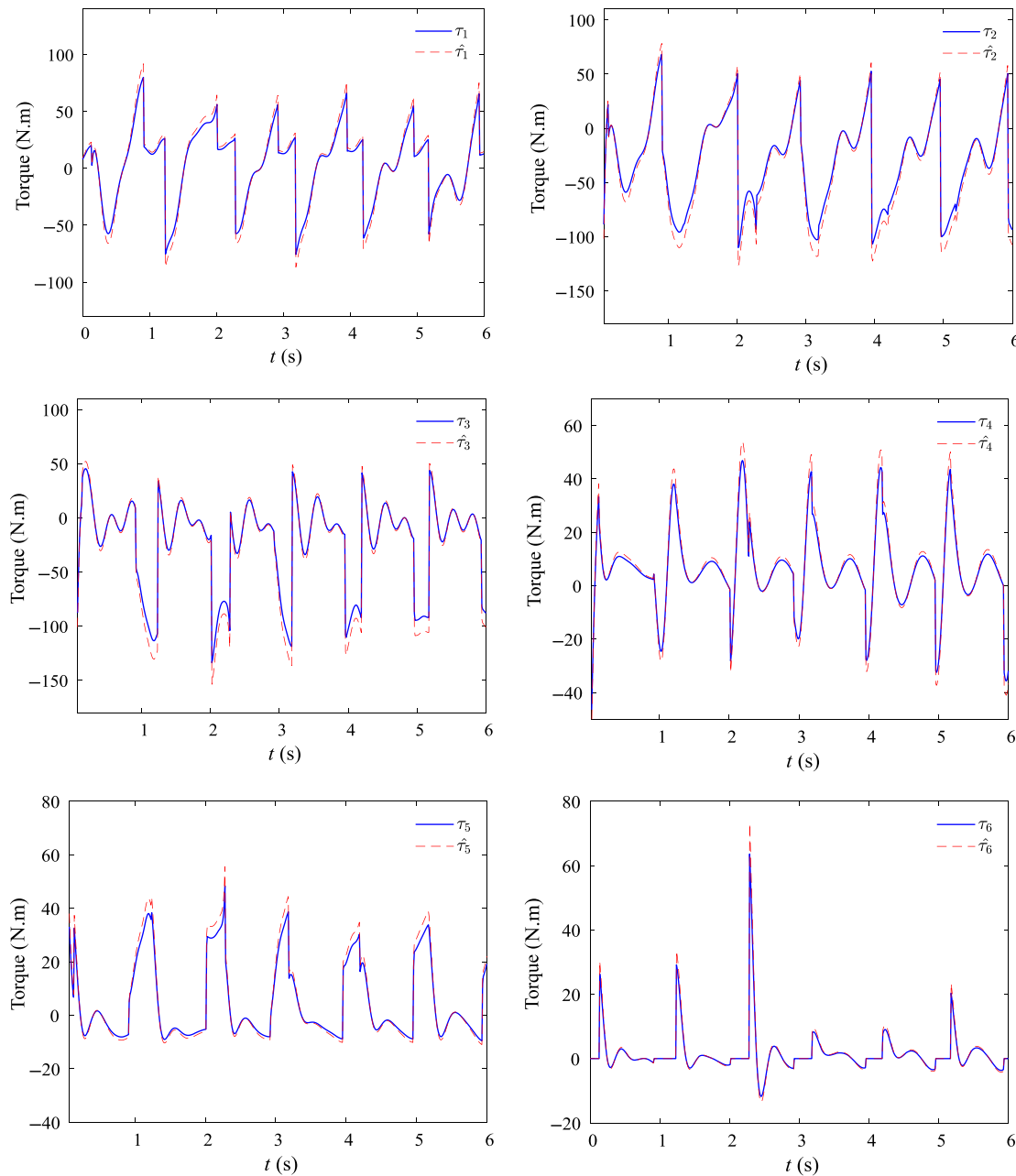| Controller | IASE (rad)$^2$ | Control signal RMS (N.M) |
|---|---|---|
| CPG-SMC | 0.0857 | 32.801 |
| ASTSMC | 0.0408 | 48.194 |
| CPG-ASTSMC | 0.0317 | 33.345 |



Fig. 8. Control command and its estimates.

and also smooth and chattering-free control command. The error between ZMP and desired ZMP for three methods, CPG-ASTSMC, CPG-SMC, and ASTSMC are 1.542, 2.248, and 3.012 m, respectively. To portray the robustness of the controller against uncertainties and disturbances, IASE criteria are shown in Fig. 11.
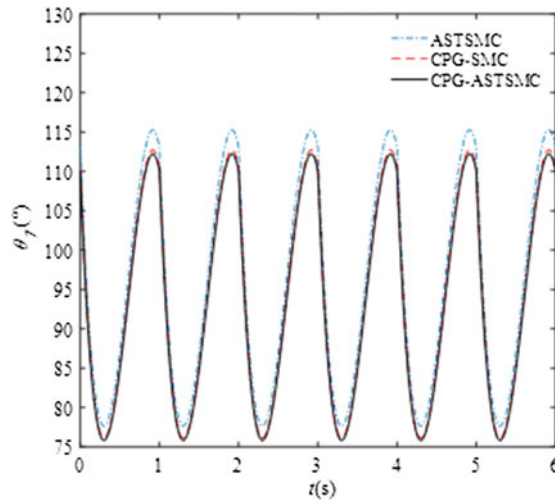
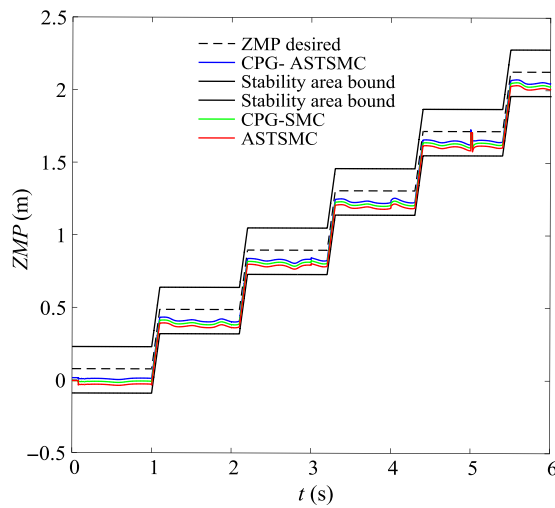Fig. 9. Desired trajectory of upper limb.
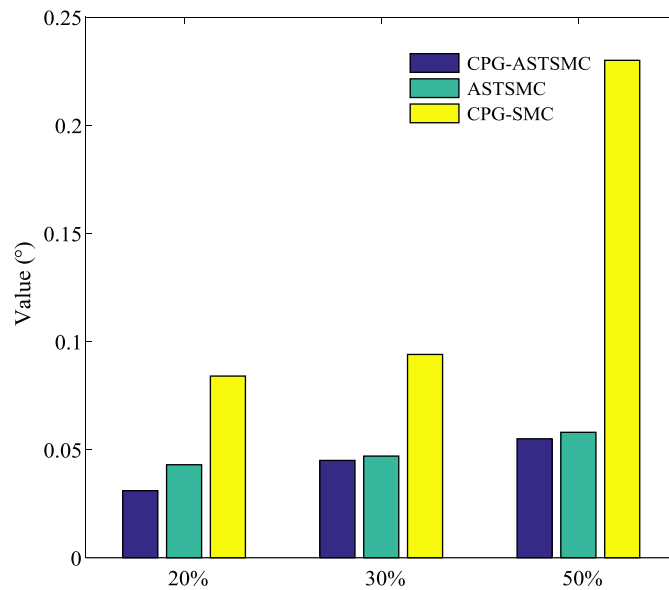


Fig. 10. The ZMP trajectory.



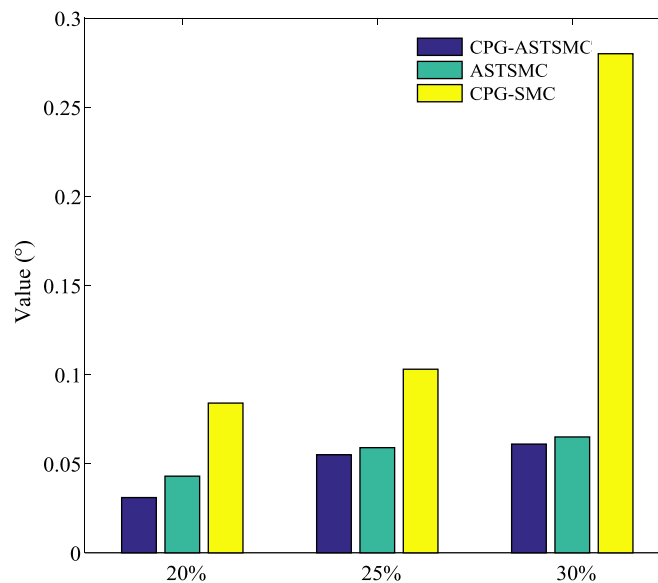Fig. 11. IASE criterion for disturbances 20, 30 and 50%.

Fig. 12. IASE criterion for three different uncertainties.

According to Fig. 11, when disturbances experience increase about 30%, all of the controller have fixed performance and for more than, CPG-SMC has weaker performance rather than others.

According to Fig. 12, when uncertainty experiences increase about 20%, all of the controller have fixed performance and for more than, CPG-SMC has weaker performance rather than others. Although the CPG-SM control method is an effective way of eliminating disturbances, but the ability of the CPG-ASTSMC and ASTSMC to simultaneously reduce the chattering phenomenon and to deal with disturbances and uncertainties with an unknown range makes it more advantageous.

## 6. Conclusion

A hybrid walking controller based on ZMP and CPG was developed in this paper which consists of two distinct sections. The first one comprises a CPG network based on coupled Vander Pol oscillators to produce stable trajectories, and the another one is the stable trajectory tracking controller. This is a reality that generating well-suited trajectories using ZMP in the realm of humanoid and walking robots are easier rather than CPG ones due to the intrinsic ability of ZMP-based methods. Although CPGs have enormous number of parameters which require to be tuned to generate the stable trajectories, but the CPG-based approaches are more robust and adaptive in comparison with ZMP-based. In order to develop and design an effective control scheme, the combination of these methods has been considered in this paper as a hybrid controller which utilizes the CPG and ZMP concepts to generate the stable trajectory profiles. In addition, to adjust the parameters of the oscillators, the parameters were bounded and then obtained accurately by HSA. Simulation results reveal adjustability of the exoskeleton with the environmental conditions and exogenous disturbances. In comparison with ASTSMC and CPG-SMC, it can be clearly seen that CPG-ASTSMC is at in highest level in terms of robustness and also performance.

## References

1. R. Bogue, "Exoskeletons and robotic prosthetics: a review of recent developments," *Indus. Robot: Int. J.* **36**(5), 421–427 (2009).
2. S. Jezernik, G. Colombo, T. Keller, H. Frueh and M. Morari, "Robotic orthosis lokomat: A rehabilitation and research tool," *Neuromodulation: Technol. Neural Interface*, **6**(2), 108–115 (2003).
3. A. Duschau-Wicke, B. Thomas, L. Lars, and R. Robert, "Adaptive support for patient-cooperative gait rehabilitation with the lokomat," **In:** *2008 IEEE/RSJ International Conference on Intelligent Robots and Systems*, (IEEE, 2008 pp. 2357–2361).
4. H. Kazerooni, R. Steger and L. Huang, "Hybrid control of the Berkeley lower extremity exoskeleton (BLEEX)," *Int. J. Robot. Res.* **25**(5–6), 561–573 (2006).
5. Springer Handbook of Robotics, (B. Siciliano and O. Khatib, eds.) (Springer, Wurzburg, 2016).
6. T. Yan, M. Cempini, C. Maria Oddo and N. Vitiello, "Review of assistive strategies in powered lower-limb orthoses and exoskeletons," *Rob. Auton. Syst.* **64**(1), 120–136 (2015).

7. Z. Qu and J. Dorsey, "Robust tracking control of robots by a linear feedback law," *IEEE Trans. Autom. Control* **36**(9), 1081-1084 (1991).

8. Y. Hong, "Finite-time stabilization and stabilizability of a class of controllable systems," *Syst. Control Lett.* **46**(4), 231-236 (2002).

9. S. T. Venkataraman and S. Gulati, "Terminal sliding modes: a new approach to nonlinear control synthesis," **In:** *Fifth International Conference on Advanced Robotics' Robots in Unstructured Environments*, Pisa, Italy (1991) pp. 443–448.

10. G. Bartolini, A. Ferrara, A. Levant and E. Usai, "On second order sliding mode controllers," **In:** *Variable Structure Systems, Sliding Mode and Nonlinear Control* (Springer, London, 1999) pp. 329–350.

11. E. F. Colet, E. F. Colet and L. M. Fridman, *Advances in Variable Structure and Sliding Mode Control*. (C. Edwards and L. Fridman, eds.) vol. 334. (Springer, Berlin, 2006).

12. A. Sabanovic, L. M. Fridman, S. Spurgeon and S. K. Spurgeon, *Variable Structure Systems: From Principles to Implementation*, vol. 66 (London, IET, 2004).

13. G. Bartolini, A. Ferrara, E. Usai and V. I. Utkin, "On multi-input chattering-free second-order sliding mode control," *IEEE Trans. Autom. Control* **45**(9), 1711–1717 (2000).

14. Y. Shtessel, C. Edwards, L. Fridman and A. Levant, *Sliding Mode Control and Observation* (Springer, New York, New York, 2014).

15. M. Zebbar, Y. Messlem, A. Gouichiche and M. Tadjine, "Super-twisting sliding mode control and robust loop shaping design of RO desalination process powered by PV generator," *Desalination* **458**, 122–135 (2019).

16. J. A. Moreno and M. Osorio, "A Lyapunov approach to second-order sliding mode controllers and observers," **In:** *2008 47th IEEE Conference on Decision and Control*, IEEE (2008) pp. 2856–2861.

17. F. Zargham and A. H. Mazinan, "Super-twisting sliding mode control approach with its application to wind turbine systems," *Energy Syst.* **10**(1), 211–229 (2019).

18. D. Liang, J. Li and R. Qu, "Super-twisting algorithm based sliding-mode observer with online parameter estimation for sensorless control of permanent magnet synchronous machine," **In:** *2016 IEEE Energy Conversion Congress and Exposition (ECCE)*, IEEE (2016) pp. 1–8.

19. Y. Shtessel, M. Taleb and F. Plestan, "A novel adaptive-gain supertwisting sliding mode controller: Methodology and application," *Automatica* **48**(5), 759–769 (2012).

20. A. Massah, A. Zamani, Y. Salehinia, M. Aliyari Sh and M. Teshnehlab, "A hybrid controller based on CPG and ZMP for biped locomotion," *J. Mech. Sci. Technol.* **27**(11), 3473–3486 (2013).

21. A. Crespi and A. J. Ijspeert, "Online optimization of swimming and crawling in an amphibious snake robot," *IEEE Trans. Rob.* **24**(1), 75–87 (2008).

22. C. Liu, Q. Chen and D. Wang, "CPG-inspired workspace trajectory generation and adaptive locomotion control for quadruped robots," *IEEE Trans. Syst. Man Cyber. Part B (Cybernetics)* **41**(3), 867–880 (2011).

23. A. J. Ijspeert, "Central pattern generators for locomotion control in animals and robots: a review," *Neural Networks* **21**(4), 642–653 (2008).

24. K. Gui, H. Liu and D. Zhang, "Toward multimodal human–robot interaction to enhance active participation of users in gait rehabilitation," *IEEE Trans. Neural Syst. Rehabil. Eng.* **25**(11), 2054–2066 (2017).

25. M. O. Ajayi, "Modelling and control of actuated lower limb exoskeletons: a mathematical application using central pattern generators and nonlinear feedback control techniques." PhD diss., Université Paris-Est (2016).

26. P. W. Latham, "A simulation study of bipedal walking robots: modeling, walking algorithms, and neural *network control*." (1992).

27. A. J. Ijspeert, "Central pattern generators for locomotion control in animals and robots: a review," Neural Networks **21**(4), 642–653 (2008).

28. A. G. Baydin, "Evolution of central pattern generators for the control of a five-link bipedal walking mechanism," *Paladyn, J. Behav. Robot.* **3**(1), 45–53 (2012).

29. M. Wang, H. Dong, X. Li, Y. Zhang and J. Yu, "Control and optimization of a bionic robotic fish through a combination of CPG model and PSO," *Neurocomputing* **337**, 144–152 (2019).

30. H. Kalani, S. Moghimi and A. Akbarzadeh, "Toward a bio-inspired rehabilitation aid: sEMG-CPG approach for online generation of jaw trajectories for a chewing robot," *Biomed. Signal Process. Control* **51**, 285–295 (2019).

31. H. Hemami and C. L. Golliday Jr., "The inverted pendulum and biped stability," *Math. Biosci.* **34**(1–2), 95–110 (1977).

32. S. Moosavian, A. Ali, K. Alipour and Y. Bahramzadeh, "Dynamics modeling and tip-over stability of suspended wheeled mobile robots with multiple arms," **In:** *2007 IEEE/RSJ International Conference on Intelligent Robots and Systems*, IEEE (2007) pp. 1210–1215.

33. A. Takhmar, M. Alghooneh, K. Alipour, S. Ali and A. Moosavian, "MHS measure for postural stability monitoring and control of biped robots," **In:** *2008 IEEE/ASME International Conference on Advanced Intelligent Mechatronics*, IEEE (2008) pp. 400-405.

34. P. N. Mousavi and A. Bagheri, "Mathematical simulation of a seven link biped robot on various surfaces and ZMP considerations," *Appl. Math. Modell.* **31**(1), 18–37 (2007).

35. M. Khalili, R. Kharrat, K. Salahshoor and M. H. Sefat, "Global dynamic harmony search algorithm: GDHS," *Appl. Math. Comput.* **228**, 195–219 (2014).

36. H. Kawamoto and Y. Sankai, "Power assist method based on phase sequence and muscle force condition for HAL," *Adv. Rob.* **19**(7), 717–734 (2005).

37. P. K. Kyaw, K. Sandar, M. Khalid, W. Juan, Y. Li, Z. Chen, Opportunities in robotic exoskeletons hybrid assistive limbSUIT (MT5009), *Robotic Exoskeletons: Becoming Economically Feasible*, Nov 21, (2013).
38. J. J. Craig, *Introduction to Robotics: Mechanics and Control, Pearson Education India* (Hall, London, 2005), pp. 85–310.
39. J. S. Bay and H. Hemami, "Modeling of a neural pattern generator with coupled nonlinear oscillators," *IEEE Trans. Biomed. Eng.* **4**(1), 297–306 (1987).
40. N. Aphiratsakun, K. Chairungsarpsook and M. Parnichkun, "ZMP based gait generation of AIT's Leg Exoskeleton," **In:** *2010 The 2nd International Conference on Computer and Automation Engineering (ICCAE)*, IEEE vol. **5**, (2010), pp. 886–890.
41. X. Yu and M. Ö. Efe, *Recent advances in sliding modes: from control to intelligent mechatronics*, vol. 24 (2015).
42. A. Levant, "Sliding order and sliding accuracy in sliding mode control," *Int. J. Control* **58**(6), 1247–1263 (1993).
43. A. Levant, "Robust exact differentiation via sliding mode technique," *Automatica* **34**(3), 379–384 (1998).
44. A. Goswami, "Postural stability of biped robots and the foot-rotation indicator (FRI) point," *Int. J. Rob. Res.* **18**(6), 523–533 (1999).